IOP Conf. Series: Materials Science and Engineering **101** (2015) 012147 doi:10.1088/1757-899X/101/1/012147

Thermal-hydraulic analysis of transients in the HELIOS loop including a CICC section representative of the JT-60SA Central Solenoid

S Carli[1], R Bonifetto[1], C Hoa[2], L Savoldi[1], R Zanino[1]

[1] NEMO Group, Dipartimento Energia, Politecnico di Torino, Corso Duca degli Abruzzi 24, 10129 Torino, Italy
[2] Univ. Grenoble Alpes, INAC-SBT, F-38000 Grenoble, France

E-mail: roberto.zanino@polito.it

Abstract. The HELIOS facility at CEA Grenoble is a supercritical helium (SHe) loop which is being used to investigate the effects on the cryogenic cooling system of the pulsed heat loads which are typical of superconducting tokamak operation. In the standard configuration, the magnet heat load is simulated by electrical heaters wrapped around a section of cryoline. In the present work, the resistively heated section is substituted in the HELIOS model of the 4C code, already validated for the standard configuration of HELIOS, by a sub-size winding structure made of JT-60SA Cable-In-Conduit Conductors (CICCs). The new model is then used to highlight the differences in the circuit behaviour when the heated pipe is substituted by an actual magnet wound with CICCs, checking the representativeness of the control strategies developed for the present HELIOS configuration. The use of CICCs will be shown to produce an intrinsic smoothing of the temperature profiles which is not affecting the capability of the control strategies to smooth the heat loads to the cryoplant.

1. Introduction

The pulsed heat load to the cryoplant is an important issue in the design and operation of tokamaks adopting superconducting (SC) magnets for the magnetic confinement, as ITER [1] or JT-60SA [2]. Indeed, the ITER refrigerators will have to withstand rapidly increasing heat loads, and not only the variations but also the power input to these refrigerators will be huge [3], requiring the over-sizing of the refrigerators to the peak load, if no smoothing strategies are adopted.

The HELIOS experimental facility [4, 5] at CEA Grenoble, France, addresses the issue of the smoothing of the pulsed heat load coming from the JT-60SA Central Solenoid (CS) to the cryoplant during plasma operation. In the experimental cryogenic loop the heat loads are applied through electrical heaters wrapped around cryolines, together mimicking the SC magnet. Different mitigation strategies have been experimentally developed, including controls acting on the thermal buffer or directly on the cryogenic circuit [6].

The 4C code [7], developed at Politecnico di Torino, is the state-of-the-art code for the thermal-hydraulic (TH) modeling of SC magnets and their cryogenic circuits. Its recent validation against experimental data from HELIOS [8] makes it able to accurately reproduce and even predict [9] the TH behavior of this experimental cryogenic loop.

Since in reality the SC magnets are composed of multi-channel Cable-In-Conduit Conductors (CICCs), whose TH detailed behavior differs from that of a heated pipe, in the present work the heated

line is substituted in the 4C HELIOS model with a suitable CICCs section representative of the JT-60SA CS. The new 4C model is then used to check if the smoothing strategies already developed at HELIOS are representative of and successful for a real magnet operation. The introduction of the CICC section in the model will also show new physical aspects that are absent in the heated pipe configuration, like the additional smoothing of the pulsed heat loads provided mainly by diffusive effects through the CICC jackets.

2. 4C HELIOS model with CICC section

The 4C model of the HELIOS loop, representative of the current experimental configuration, is reported in Figure 1a, and its main details are available in [8, 10, 11]. Different controls are present in the experimental loop, like the one considered here that regulates the cold circulator speed by monitoring the FE4 mass flow rate.

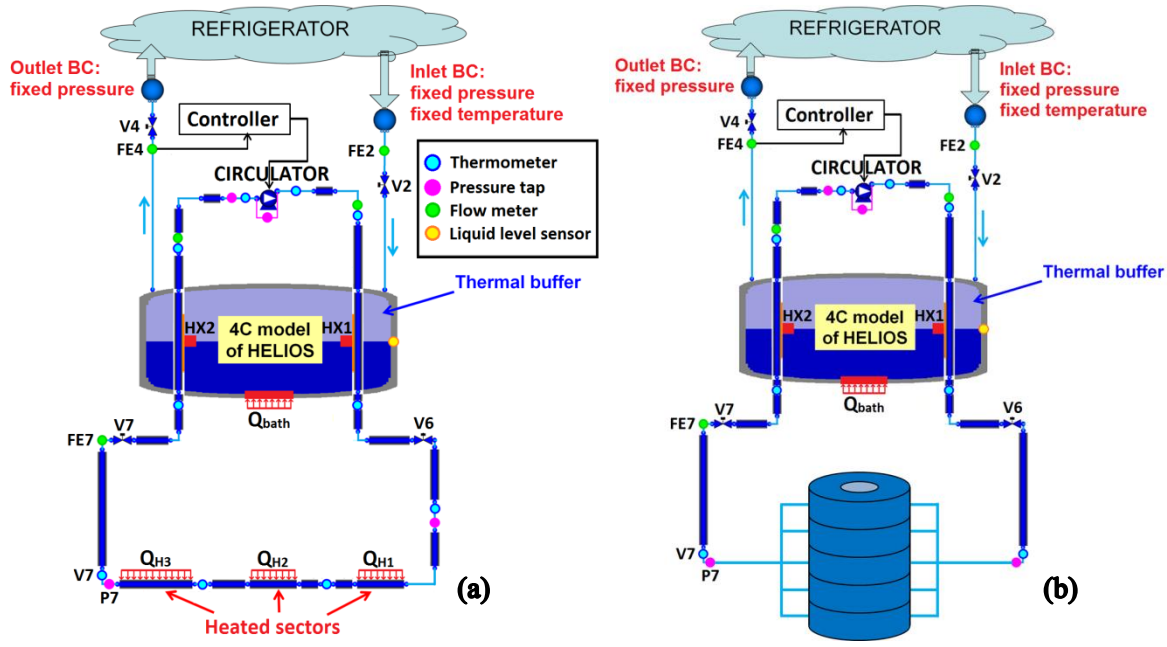

Figure 1. 4C model of HELIOS (a) with heated line; (b) with CICC section.

In the new 4C model of the HELIOS loop, the heated line is substituted with a CICC winding pack (WP), see Figure 1b, constituted by five CICCs in parallel, representative of the JT-60SA CS in the following sense: the total mass flow rate (32 g/s) and He volume (0.08 m^3) inside the heated line are kept constant in the multi-channel section, as it can be seen from Table 1, and equal to 1/20 of the JT-60SA CS values – this constraint reflects the scaling factor used for the entire HELIOS loop. The flow area of the heated line, having the same length of a JT-60SA CS hydraulic channel, was designed in order to comply with the above-mentioned constraint (1/20 scale ratio); to keep the transit time in the heated section equal to the current configuration, 5 parallel, full length CICCs are required, as reported in Table 1. The overall pressure drop on the CICC section is ~0.7 bar with valve V7 fully open. In order to keep the same total mass flow rate inside the circuit, the pump speed must be increased to 8290 rpm with respect to the nominal 7866 rpm of the heated line configuration, to compensate the slightly higher pressure drop in the CICCs with respect to the heated line configuration, where most of the pressure drop was induced by V7.

A controller is also active on the thermal buffer, controlling FE4 mass flow rate acting on V4 valve opening (FE4 set point 21.3 g/s).

Table 1. Parameters of the heated line and CICC section**.**

	Heated line	CICC section
Inner diameter (mm)	30.5	Bundle: 21 Central channel: 7
Length (m)	107	107
Helium volume (m^3)	0.08	0.08
# of channels in parallel	1	5
Mass flow rate per channel (g/s)	32	6.4

The JT-60SA CS CICC cross section adopted for the present work is schematically shown in Figure 2, with the additional data listed in Table 2.

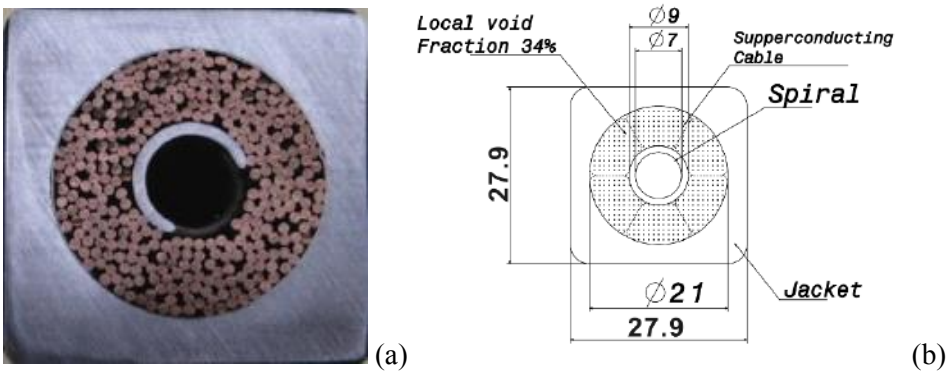

(a) (b)

Figure 2. JT-60SA CS conductor cross section: (a) picture (reproduced from [12]) and (b) sketch with dimensions (courtesy of CEA).

Table 2. Parameters of the JT-60SA CS conductor [2]**.**

Type of strand	Nb_3Sn
Inlet temperature (K)	4.4-4.6
Jacket material	SS316LN
SC strand diameter (mm)	~0.82
SC strand Cu:non-Cu	~1.0
Cabling pattern	3x3x6x6
SC strand number	~216
Cu wire number	~108
Insulation material	Glass epoxy
Insulation thickness (mm)	Inter-turn: 1.24 Inter-pancake: 1.54

A single hydraulic channel of the CICC section is constituted by a double pancake of 22 turns, see Figure 3, with inlet and outlet positioned both on the outboard side of the WP. The whole CICC section is shown in Figure 4. It can be seen that the double pancakes are arranged in such a way that neighboring CICCs have the inlet or outlet paired, thus having a counter current flow on adjacent double pancakes, and, consequently, a non-symmetric dynamic behaviour.

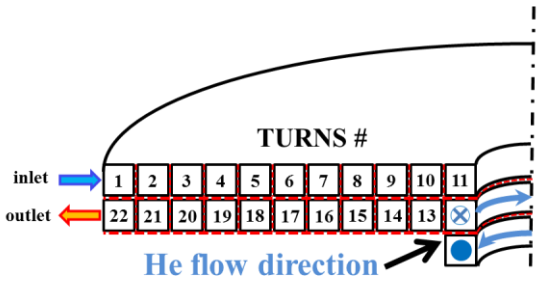

Figure 3. Single CICC with detail of the He flow direction: fluid entering the page plane is represented by a dot with a cross, while fluid exiting from the page plane is represented with a full dot. The conductor insulation is represented with dashed lines.

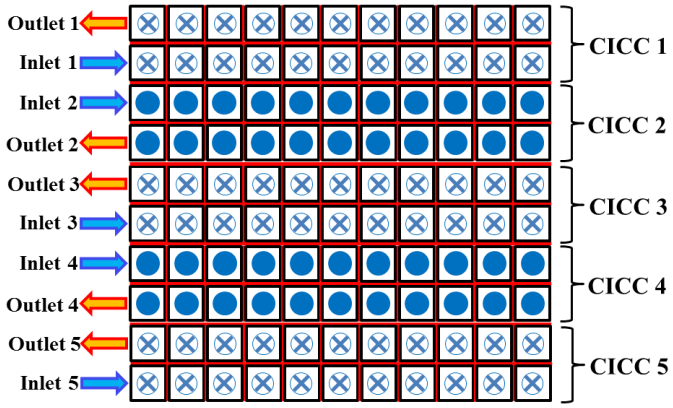

Figure 4. Five CICC in parallel with details of fluid flow direction and inlet/outlet pairing between adjacent channels.

The thermal coupling among neighboring CICCs is accounted for in the 4C model, between both turns and pancakes, as it can be seen from Figure 5. This feature will be shown in the following section to produce an intrinsic smoothing of the heat loads, not present in the heated line configuration.

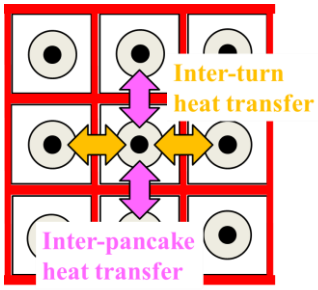

Figure 5. Zoom of the CICC cross section with details of inter-turn and inter-pancake heat transfer.

3. Results

Three different cases are considered: in case A, the main differences in the dynamic behavior introduced by the CICC with respect to the heated line are presented. In case B the effect of a heat load non-uniformly distributed both on turns and channels is studied, in comparison with a uniform heat distribution. In case C, a controlled scenario is presented for the smoothing of the heat loads to

the cryoplant, with uniform power distribution on the CICC section, in order to check the adequacy of the control strategy previously developed in the HELIOS heated line configuration.

3.1. Case A

In this first case, the standard HELIOS configuration with heated line is compared with the new one, containing a CICC section, for the same given heat load scenario.

The driver used here is a single 50 s pulse, in which 150 W are deposited in each heater of the heated line, according to the spatial distribution reported in Figure 6a, considering a single axial coordinate starting from T6, see figure 1a. For the sake of comparison, in the CICC configuration, a simulation has been performed with the same heat load spatial profile as in the heated line, deposited in the jacket of each CICC, see again Figure 6a.

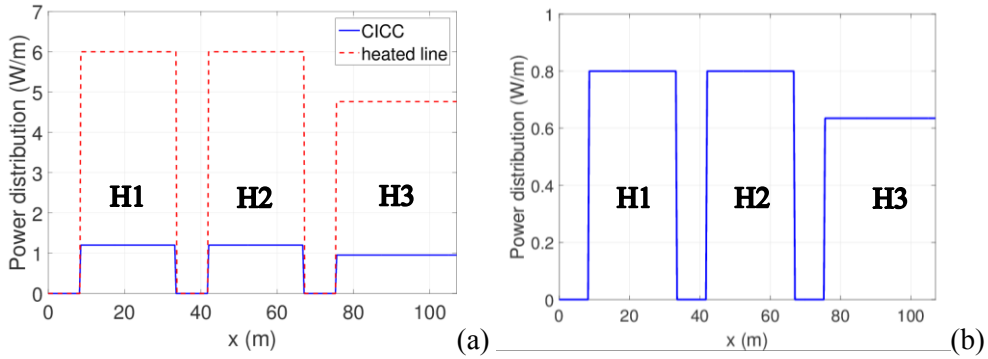

Figure 6. (a) Power distribution in each CICC of the CICC section (solid line) and in the heated line (dashed line) in case A; (b) power distribution along each CICC for case C.

In Figure 7a we present the evolution of the temperature at the outlet of the heated line (or CICC section), i.e. at the location of the T7 sensor. We consider first a case with negligible inter-turn and inter-pancake thermal coupling (so-called adiabatic – AD – condition). The computed results are reported in Figure 7a and show a smoother profile, with respect to the heated line, with lower temperature peaks (which are due to the three, spatially separated, heaters inside the heated line [8]), due to the heat diffusion along and across the CICC (jacket and strands). When inter-turn and inter-pancake heat transfer is active, the T7 profile is even more smoothed than in adiabatic condition, with a single peak and no undershoot, due to the combination of heat diffusion inside the solids and heat transfer between turns and pancakes, see again Figure 7a.

In Figure 7b the computed pressure profile at the outlet of the heated line (or CICC section), i.e., at the P7 location, is reported. In the ramp-up phase the configuration with CICCs, both in adiabatic and coupled conditions, shows a behaviour similar to the heated line, with a lower peak due to lower T7 (see Figure 7a). In the ramp-down phase the coupled CICC condition presents no sub-cooling effect, again following the T7 profile, as opposed to what was seen with the heated line.

3.2. Case B

In case B the standard JT-60SA input power scenario [11, 13] is adopted, with the waveform shown in Figure 8a. A non-uniform distribution of the heat load is chosen for the CICC section which follows a realistic magnetic field distribution inside the CS, see Figure 8b. Therefore, the central CICC (#3) is more loaded than the two adjacent ones, which, on their own, are more loaded than the two top and bottom CICCs. Moreover, along each CICC the power distribution grows turn by turn, from the outboard to the inboard, following an almost triangular profile peaked in the middle of the hydraulic channel length (inboard turns), see again Figure 8b.

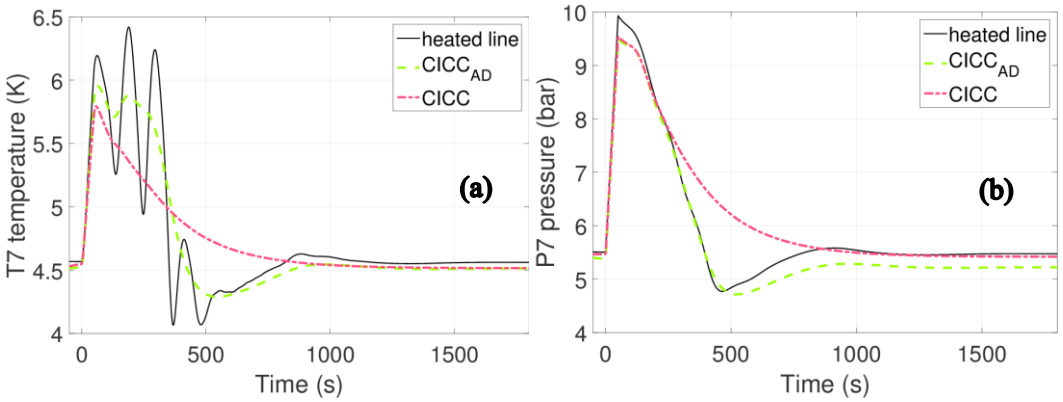

Figure 7. Case A: (a) temperature at T7 and (b) pressure at P7 evolution for the heated line (solid thin line), the adiabatic CICC (dashed thick line) and the coupled CICC (dash-dotted thick line) configurations.

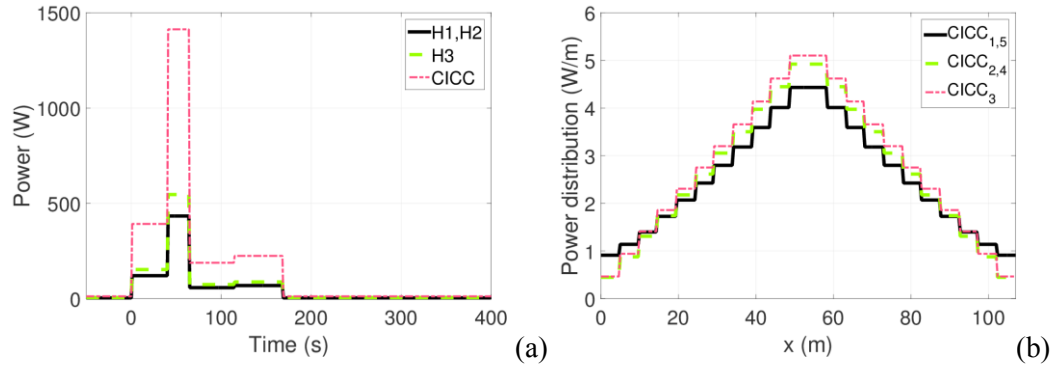

Figure 8. Case B: (a) Evolution of the heat load, in the heaters *H1-H2* (solid thick line) and *H3* (dashed thick line) of the heated line, and the corresponding total input power to the CICC section (dash-dotted thin line); (b) distribution of the heat load along $CICC_1$ and $CICC_5$ (solid thick line), $CICC_2$ and $CICC_4$ (dashed thick line) and $CICC_3$ (dash-dotted thin line) at time $t = 50$ s.

Figure 9a reports the computed T7 temperature evolution for the standard heated line configuration and for the new CICC configuration, driven by both a uniform and non-uniform power distribution. The main outcome here is that there are negligible differences between the dynamic evolution of T7 in case of uniform and non-uniform distribution of the heat loads inside the CICC section, with only a slightly higher and delayed peak in the non-uniform case. This implies a negligible effect of the non-uniform heat load distribution on the smoothing capability.

In Figure 9b the evolution of the mass flow rate at the inlet and outlet of the CICCs is presented. As expected, the more a CICC is loaded, the stronger is the helium expulsion at the outlet and the mass flow rate reduction at the inlet.

Note that, as a byproduct of this simulation, the computed temperature profile along each CICC, see Figure 10, shows a clear peak in the middle, driven by the magnetic field profile which in turns would drive the heat load (to be expected in the form of AC losses for the CS), which confirms the concern for the coil operation [14]. Indeed, if this behavior will be confirmed in a full scale model coil, as the peak operating temperature is computed at the inboard turns, i.e. at the location of the minimum T_{CS} value, the temperature margin would be reduced.

3.3. Case C

In the final case studied here, a controlled scenario, already shown to be successful in the current HELIOS configuration [9], is applied to the new HELIOS configuration with the CICC WP. The control is actuated by a proportional-integral (PI) controller, which regulates the pump speed on the basis of the vapor mass flow rate to the refrigerator (FE4), see Figure 1 and Table 3. The driver of the scenario consists of a uniform heat load (according to the heated sections of the heated line) along the CICCs, as shown in Figure 6b.

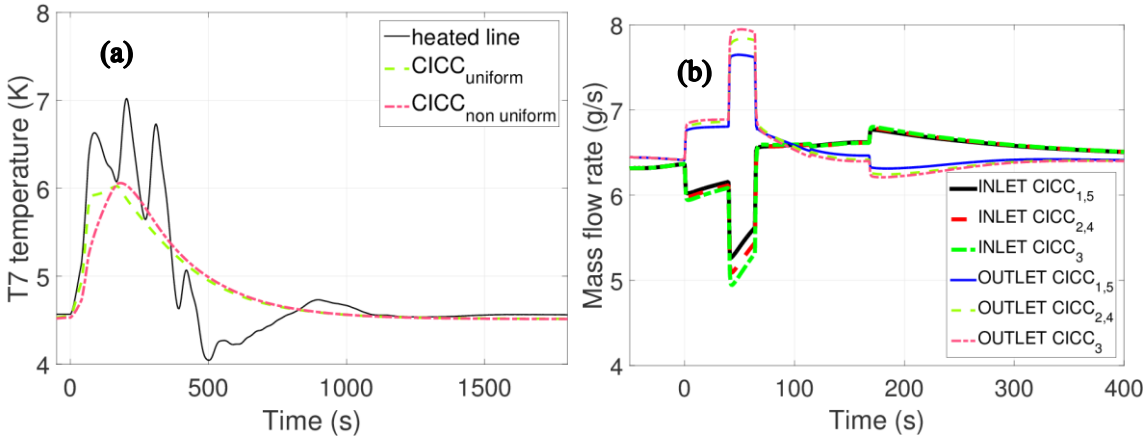

Figure 9. Case B: (a) T7 temperature evolution for the heated line (solid thin line), the uniform load distribution with CICC (dashed thick line) and non-uniform load distribution with CICC (dash-dotted thick line) configurations, and (b) evolution of the mass flow rate at the inlet and outlet of the CICCs in the case of non-uniform distribution of the heat load.

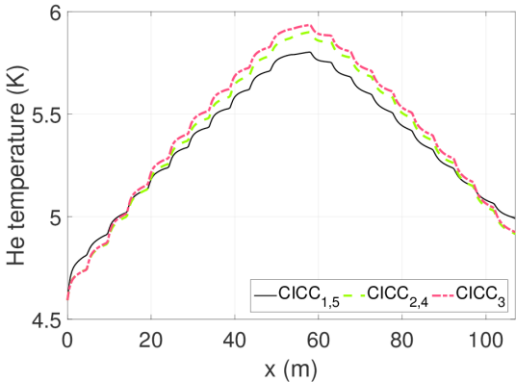

Figure 10. Case B: He temperature distribution along the CICCs at time t = 50 s.

Table 3. Parameters of the PI controller**.**

Set point	14.5 g/s
Gain *Kp*	$4.8 \cdot 10^5$
Integrator time *Ti*	4 s
Minimum output	3305 rpm
Maximum output	8290 rpm

The results of the controlled scenario are compared to the very same scenario without any control, to check the effect of the smoothing strategy.

In Figure 11a, the evolution of the actuator (pump speed) and of the controlled variable (FE4 mass flow rate) are reported. As soon as FE4 overcomes the set-point, the pump speed starts decreasing. In

the same way FE7 decreases, significantly contributing to the smoothing of the heat load to the cryoplant, see Figure 11b. The oscillations seen in the evolution of the power to the refrigerator in controlled scenario are due to the oscillation of the pump speed and thus of FE7.

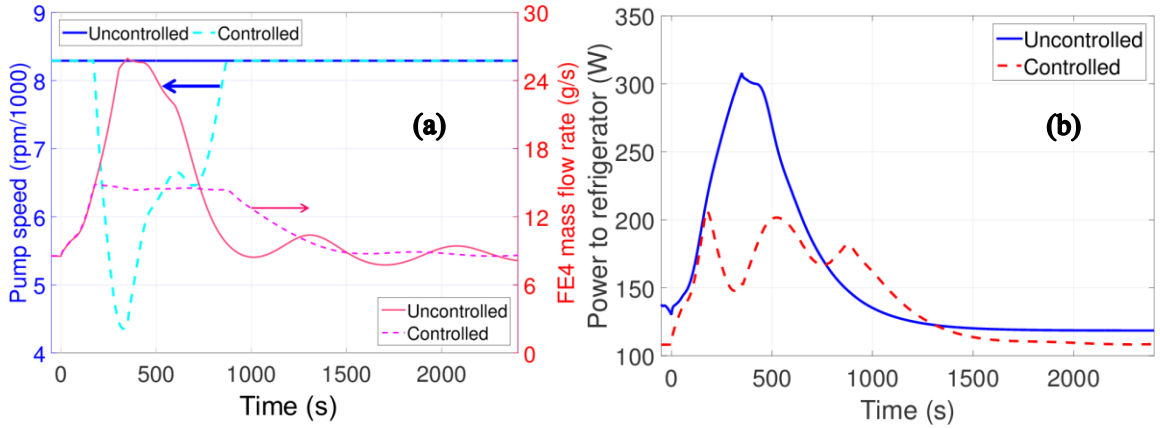

Figure 11. Case C: (a) Evolution of the pump speed (left axis, thick lines) and of the FE4 mass flow rate (right axis, thin lines) and (b) evolution of the power released to the refrigerator in the uncontrolled (solid lines) and controlled (dashed) scenarios.

4. Conclusions and perspective

The comparison between the 4C HELIOS heated line model with the new 4C model with a CICC section, representative of the JT-60SA CS, has been carried on.

The use of CICCs has been shown to produce an intrinsic smoothing of the temperature profiles (in case of both uniform and non-uniform heating) due to heat diffusion in the CICC and to both inter-turn and inter-pancake thermal coupling. As a result, the pulsed heat loads are less severe with respect to the heated line configuration.

The smoothing strategies successfully developed in the standard HELIOS configuration (with a simple resistively heated line), e.g., based on the regulation of cold circulator speed, are also successful in the case of the CICC configuration.

References

[1] Mitchell N et al. 2012 *IEEE Trans. Appl. Supercond.* **22** 4200809
[2] Zani L et al. 2011 *IEEE Trans. Appl. Supercond.* **21** 1938-1943
[3] Kuendig A and Schoenfeld H 2006 Helium refrigerator design for pulsed heat load in tokamaks *Adv. Cryo. Eng.*1995-2001
[4] Hoa C et al., 2010 *Proceedings of the 23rd International Cryogenic Engineering Conference (ICEC23)*
[5] Hoa C et al. 2012 *Cryogenics* **52** 340-348
[6] Lagier B et al. 2014 *AIP Conference Proceedings* **1573** 1602-1609
[7] Savoldi Richard L et al. 2010 *Cryogenics* **50** 167-176
[8] Zanino R et al. 2013 *Cryogenics* **53** 25-30
[9] Zanino R et al. 2014 *AIP Conference Proceedings* **1573** 1586-1593
[10] Bonifetto R et al. 2012 *AIP Conference Proceedings* **1434** 1743-1750
[11] Zanino R et al. 2013 *Cryogenics* **57** 31-44
[12] Available: www.jt60sa.org (accessed on June 28, 2015)
[13] Guelfi F et al. 2014 *Cryogenics* **64** 51-62
[14] Martovetsky N 2015 *Private communication*